



|                  |  |
|------------------|--|
| Title            | Irradiation-tolerant lung cancer cells acquire invasive ability dependent on dephosphorylation of the myosin regulatory light chain        |
| Author(s)        | Ishihara, Seiichiro; Yasuda, Motoaki; Nishioka, Takeshi; Mizutani, Takeomi; Kawabata, Kazushige; Shirato, Hiroki; Haga, Hisashi            |
| Citation         | FEBS Letters, 587(6), 732-736<br><a href="https://doi.org/10.1016/j.febslet.2013.01.055">https://doi.org/10.1016/j.febslet.2013.01.055</a> |
| Issue Date       | 2013-03-18   |
| Doc URL          | <a href="http://hdl.handle.net/2115/52653">http://hdl.handle.net/2115/52653</a>  |
| Type             | article (author version)   |
| File Information | Ishihaga_FEBS_587_p732.pdf   |



[Instructions for use](#)

**Irradiation-tolerant lung cancer cells acquire invasive ability  
dependent on dephosphorylation of the myosin regulatory light chain**

Seiichiro Ishihara<sup>a</sup>, Motoaki Yasuda<sup>b</sup>, Takeshi Nishioka<sup>c</sup>, Takeomi Mizutani<sup>a</sup>, Kazushige Kawabata<sup>a</sup>, Hiroki Shirato<sup>d</sup>, and Hisashi Haga<sup>a,\*</sup>

<sup>a</sup>Transdisciplinary Life Science Course, Faculty of Advanced Life Science, Hokkaido University, N10-W8, Kita-ku, Sapporo 060-0810, Japan

<sup>b</sup>Department of Oral Pathobiological Science, Graduate School of Dental Medicine, Hokkaido University, N13-W7, Kita-ku, Sapporo 060-8586, Japan

<sup>c</sup>Department of Biomedical Sciences and Engineering, Faculty of Health Sciences, Hokkaido University, N12-W5, Kita-ku, Sapporo 060-0812, Japan

<sup>d</sup>Department of Radiology, Hokkaido University Graduate School of Medicine, N15-W7, Kita-ku, Sapporo 060-8638, Japan

**\* To whom correspondence should be addressed:**

H. Haga

Transdisciplinary Life Science Course, Faculty of Advanced Life Science, Hokkaido University, N10-W8, Kita-ku, Sapporo 060-0810, Japan

Tel: +81 11 706 4909

Fax: +81 11 706 4909

E-mail address: [haga@sci.hokudai.ac.jp](mailto:haga@sci.hokudai.ac.jp) (H. Haga).

**ABSTRACT**

Radiotherapy is one of the major treatment modalities for malignancies. However, cells surviving irradiation often display high levels of invasiveness. This study shows that irradiation-tolerant lung adenocarcinoma demonstrates high invasive capability depending on dephosphorylation of the myosin regulatory light chain (MRLC). In a collagen gel overlay condition, low-invasive subclones of lung adenocarcinoma (A549P-3) showed a round morphology and diphosphorylation of MRLC. In contrast, irradiation-tolerant A549P-3 cells (A549P-3IR) displayed high invasiveness and a lower level of MRLC diphosphorylation. In addition, inhibition of MRLC phosphatase activity decreased the invasive activity. These findings suggest that A549P-3IR cells acquire high invasiveness through MRLC dephosphorylation.

*Keywords:*

3D culture; collagen gel; irradiation; invasion; lung adenocarcinoma; myosin regulatory light chain

**HIGHLIGHTS**

- Low-invasive cancer cells show diphosphorylation of myosin regulatory light chain.
- High-invasive cancer cells show dephosphorylation of myosin regulatory light chain.
- Diphosphorylation of myosin regulatory light chain inhibits malignant cell invasion.

## 1. Introduction

Radiotherapy is often the primary treatment for many types of malignancies. However, it has been reported that growth and metastasis of solid tumors are induced after local tumor irradiation [1]. Recent studies have revealed that some cancer cells show higher motility and invasiveness after irradiation than prior to irradiation [2, 3]. It has also been reported that irradiation of cancer cells leads to increased expression of adhesion molecules, integrins [4, 5], or matrix metalloproteinases [6]. These findings indicate that irradiation of tumors can evoke malignant properties, although the details of the underlying mechanism is not well understood.

Contractile force is important for many physiological functions such as cell migration, cytokinesis, and morphological change. Contractile force is generated by the contractility mediated by actomyosin, composed of actin filaments and myosin II. In this process, the myosin regulatory light chain (MRLC) is essential for myosin motor activity, and phosphorylation of Ser19 and/or Thr18 of MRLC is crucial for its activation [7]. Contractile forces also play an important role in cell migration on a 2D substrate. MRLC diphosphorylation induced by RhoA-dependent ROCK activity triggers cellular contractile forces [8, 9]. On the other hand, in a 3D environment, the relationship between cell migration and cellular contractile forces is not well studied.

In this study, we investigated the contribution of contractile forces generated by

diphosphorylation of MRLC to the invasive behavior of irradiation-tolerant cancer cells in a 3D environment. Our previous study revealed that irradiation-tolerant lung adenocarcinoma cells show integrin  $\beta$ 1-dependent invasive activity in a 3D collagen matrix [10]. We show here that high-invasive irradiation-tolerant lung cancer cells demonstrate a lower level of MRLC diphosphorylation than that of low-invasive lung cancer cells in a 3D collagen matrix, and that the invasiveness is dependent on integrin  $\beta$ 1 activity. We also show that constitutive phosphorylation of MRLC, by use of a phosphatase inhibitor, decreases the invasive activity of irradiation-tolerant cells.

## **2. Materials and Methods**

### *2.1. Cell culture*

The lung adenocarcinoma A549 cell line was purchased from the American Type Culture Collection (ATCC; Manassas, VA). A subclonal A549 cell line (P-3) and irradiation-tolerant P-3 cell line (IR) were established, as previously reported [10]. Cells were cultured in Dulbecco's Modified Eagle's Medium (DMEM; Sigma, St. Louis, MO) supplemented with 10% fetal bovine serum (FBS; JRH Biosciences Inc., Lenexa, KS) and 1% antibiotic/antimycotic solution (Invitrogen, Carlsbad, CA). Cells were incubated at 37°C in a humidified incubator with 5% CO<sub>2</sub>.

### *2.2 Reagents*

We used Y27632 (Sigma) to inhibit Rho kinase (ROCK) activity and to reduce MRLC phosphorylation. We used calyculin A (CA; Sigma) to inhibit phosphatase activity of myosin light chain phosphatase (MLCP) [11]. To inhibit integrin  $\beta$ 1 activity, we used monoclonal antibody AIIB2 [12] (purchased from the Developmental Studies Hybridoma Bank at the University of Iowa). We used rat serum IgG (I8015, Sigma) as a control antibody. We made a 1.6 mg/mL collagen type I gel with Cellmatrix Type I-P (Nitta Gelatin Inc., Osaka, Japan). For immunofluorescence staining of F-actin, AlexaFluor-488 phalloidin (Invitrogen) was used at a

1:1000 dilution. Phospho-myosin light chain 2 (Ser19/Thr18) antibody (#3674; Cell Signaling Technology, Beverly, MA) was used as a primary antibody for staining of diphosphorylated MRLC (PP-MRLC) at a 1:150 dilution. AlexaFluor-594 goat anti-rat IgG (H + L; Invitrogen) was used as a secondary antibody for PP-MRLC staining at a 1:500 dilution.

### *2.3. Immunofluorescence staining*

A glass dish of 8.0 mm radius was filled with 100  $\mu$ L of collagen gel and  $4 \times 10^3$  cells were seeded onto the collagen gel. After 24 h, 50  $\mu$ L of collagen sol were poured on the dish and incubated at 37°C for 30 min for gelation. This method allowed the cells to be cultured in a 3D substrate. After 24 h, cells were fixed with 4% paraformaldehyde in PBS for 10 min, permeabilized with 0.5% Triton X-100 in PBS for 10 min, and blocked with 5% skim milk in PBS for 1 h. For PP-MRLC staining, cells were incubated overnight with the primary antibody in 0.5% skim milk in PBS at room temperature. Then, the cells were rinsed 3 times with 0.5% skim milk in PBS and incubated with secondary antibody in 0.5% skim milk in PBS for 1 h at room temperature. After reaction with secondary antibody, cells were rinsed 3 times with 0.5% skim milk in PBS. Fluorescence images were obtained using confocal laser scanning microscopy (C1 confocal imaging system; Nikon Instech., Tokyo, Japan). To analyze the relative PP-MRLC fluorescence intensity, we calculated fluorescence intensity and analyzed the

intensity ratio of PP-MRLC per F-actin by Image-Pro software (Media Cybernetics Inc., Silver Spring, MD).

#### *2.4. Roundness index analysis*

A glass dish of 12.5 mm radius was filled with 250  $\mu$ L of collagen gel, and  $1 \times 10^4$  cells were seeded onto the collagen gel. After 24 h, 125  $\mu$ L of collagen sol was poured on the dish and incubated at 37°C for 30 min for gelation. Then, the cells were incubated with or without Y27632 (20  $\mu$ M), CA (1 nM), or AIB2 (30 ng/ml) at 37°C. After 24 h, cells were fixed with 4% paraformaldehyde in PBS for 10 min and permeabilized with 0.5% Triton X-100 in PBS for 10 min. For F-actin staining, the cells were incubated with AlexaFluor-488 phalloidin in PBS for 20 min at 37°C. Then, the cells were rinsed 3 times. Fluorescence images were obtained by confocal laser scanning microscopy and the roundness index was calculated using Image-Pro software, as previously reported [10].

#### *2.5. Time-lapse observation*

A glass dish of 12.5 mm radius was filled with 1000  $\mu$ L of collagen gel, and  $1 \times 10^4$  cells were seeded onto the collagen gel. After 24 h, 500  $\mu$ L of collagen sol were poured onto the dish and incubated at 37°C for 30 min for gelation. Then, the dish was filled with culture

medium and sealed with silicone grease to avoid exposure to air and a change in the pH of the media. A phase-contrast microscope (TE300, Nikon Instech.), equipped with a 10 × objective and a 37°C acrylic resin incubation box, was used for time-lapse observations of cells. Image-Pro software was used for time-lapse observation, which involved capturing images every 5 min. After 12 h, the cells were treated with CA at a concentration of 1.5 nM and the observation was continued. After 12 h, we removed the media and washed the cells 3 times with fresh DMEM to remove CA from the dish. The observation was continued for 27 h after removing CA. The movie was edited from a series of the captured images.

## *2.6 Statistical analysis*

Mean and standard deviation (SD) of fluorescence intensities were calculated, and statistically significant differences were identified using Student's *t*-tests.

### 3. Results

#### 3.1. *Diphosphorylation level of MRLC in P-3 and IR cells*

To investigate differences in the contractile force between low-invasive subclonal A549 lung adenocarcinoma cells (P-3) and high-invasive irradiation-tolerant P-3 cells (IR) cultured in a 3D collagen gel matrix, we performed immunofluorescent staining of diphosphorylated MRLC (PP-MRLC). PP-MRLC intensity in IR cells was higher than that of P-3 cells (Fig. 1A). Analysis of the PP-MRLC fluorescence intensities indicated that the PP-MRLC intensity in P-3 cells was significantly higher than that in IR cells (Fig. 1B). The SD of intensities (shown as error bars in Fig. 1B) in P-3 cells was larger than that in IR cells. This is because some of P-3 cells had low PP-MRLC fluorescence intensity, whereas that in IR cells consistently demonstrated low PP-MRLC fluorescence intensity. These results suggested that high-invasive IR cells consistently generate lower contractile force compared to low-invasive P-3 cells.

#### 3.2. *Spindle morphology induced by dephosphorylation of MRLC in P-3 cells*

We treated P-3 cells with Y27632, an inhibitor of MRLC phosphorylation, and observed the morphological changes in a 3D matrix. Treatment with Y27632 significantly reduced PP-MRLC fluorescence intensity in P-3 cells (Fig. S1). Analysis of roundness index

revealed that most of the untreated P-3 cells showed a round morphology in a collagen gel. In contrast, a significant number of P-3 cells treated with Y27632 displayed spindle morphology (Figs. 2A, B). These results suggested that dephosphorylation of MRLC induces invasive morphology in P-3 cells cultured in a 3D matrix.

### *3.3. Invasive behavior induced by diphosphorylation of MRLC in IR cells*

Next, we promoted diphosphorylation of MRLC in IR cells with CA, known to be an inhibitor of protein phosphatase [11], and observed the morphological changes. IR cells treated with CA showed a higher intensity of PP-MRLC immunofluorescence than did untreated IR cells in a collagen gel (Fig. S2). Roundness index indicated that the proportion of IR cells with a round morphology after treatment with CA was significantly greater than that in untreated IR cells in a 3D matrix (Fig. 2C, D).

We also observed the invasive behavior of IR cells in a 3D matrix. Under untreated condition, IR cells displayed spindle morphology and invaded in a 3D collagen gel (Fig. 3, Movie; Supplementary material). However, after CA treatment, IR cells changed to a round morphology, and showed reduced invasiveness. Furthermore, after washout treatment, IR cells recovered to a spindle morphology and demonstrated higher invasiveness. These results indicated that dephosphorylation of MRLC is essential for high invasive activity in IR cells.

### *3.4. Activity of integrin $\beta 1$ is essential for spindle morphology*

We previously reported that spindle morphology of IR cells in a 3D collagen matrix is dependent on integrin  $\beta 1$  activity [10]. We here investigated the contribution of integrin  $\beta 1$  activity to the morphological change in P-3 cells to a spindle shape induced by dephosphorylation of MRLC. Roundness index indicated that the majority of P-3 cells treated with both Y23632 and AIIB2, an inhibitory monoclonal antibody, showed a round morphology (Fig. 4A, B). On the other hand, most of the P-3 cells treated with only Y27632 showed a spindle morphology. Treatment with a control antibody did not induce morphological changes to the round morphology of P-3 cells treated with Y27632 (Fig. S3). These results indicated that the activity of integrin  $\beta 1$  is necessary for the spindle morphology that is induced by MRLC dephosphorylation in P-3 cells.

#### 4. Discussion

This study showed that MRLC dephosphorylation induces spindle morphology and a high-invasive phenotype in A549 lung adenocarcinoma cells. Low-invasive P-3 cells showed a round morphology that was dependent on PP-MRLC in a 3D collagen gel. On the other hand, irradiation-tolerant IR cells displayed high levels of invasive activity and a spindle morphology that was dependent on dephosphorylation of MRLC. The relationship between MRLC phosphorylation and the invasive behavior of irradiation-tolerant cancer cells has not been reported previously.

Because PP-MRLC generates strong contractile forces in actomyosin [7], the low invasiveness of P-3 cells in a 3D matrix is probably due to the strong contractile forces of actomyosin. We speculate that the inward contractile forces at the cell periphery maintain a round morphology and prevent protrusions from the cell surface. On the other hand, a previous report suggested that contractile forces are necessary for cancer cells to pull the cell body in the direction of migration [13]. Our results indicate that excessive contractile force prevents the invasive activity of P-3 cells.

In addition to MRLC, integrin  $\beta$ 1 also contributes to the invasive activity in P-3 and IR cells. In this study, we showed that P-3 cells treated with Y27632 demonstrate an invasive phenotype that is dependent on integrin  $\beta$ 1 activity. In addition, we previously reported that

inhibition of integrin  $\beta 1$  activity prevents an invasive phenotype in IR cells [10]. Another study showed that HT1080 fibrosarcoma cells overexpressing MT1 matrix metalloproteinase show an invasive phenotype in a 3D collagen matrix that is dependent on integrin  $\beta 1$  activity [14]. Collectively, integrin  $\beta 1$  activity may be essential for various types of cancer cell to invade in a 3D matrix.

MRLC is a possible therapeutic target in malignant lung adenocarcinoma for preventing invasion. In this study, we showed that CA treatment increases the phosphorylation level of PP-MRLC and inhibits the invasive activity of IR cells in a collagen gel. Thus, CA may be a possible therapeutic agent against malignant lung adenocarcinoma. We also showed that Y27632 treatment triggers dephosphorylation of MRLC and induces an invasive phenotype in P-3 cells. This result indicates that Y27632 treatment may facilitate the progression of lung adenocarcinoma. On the other hand, a previous study showed that Y27632 treatment prevented the progression of invasive hepatoma *in vivo* [15]. From these results, we suggest that both CA and Y27632 have a potential as therapeutic reagents against cancer cells, although the effects of these reagents seem to depend on the type of cancer cells.

We also suggest a new therapy that targets MRLC in normal tissue cells after radiotherapy. Radiotherapy damages not only tumor tissues but also normal tissues. Wound healing, including migration of fibroblasts, is a key process for repairing normal tissues

damaged by irradiation. However, irradiation disrupts the activity of fibroblasts, including migration, and perturbs the repair process of normal tissues after radiotherapy [16, 17]. A previous study showed that myosin II activity is essential for the migration ability of fibroblasts [18]. Because myosin II activity is decreased by dephosphorylation of MRLC, this dephosphorylation may decrease the migration ability of fibroblasts, in comparison to that of IR cells. Thus, we speculated that irradiation prevents migration of fibroblasts via dephosphorylation of MRLC, and as a result, inhibits the wound-healing process. A previous study reported that CA treatment of fibroblasts increases mono- or di-phosphorylated MRLC [19]. Therefore, CA may help recover migration ability via MRLC phosphorylation in irradiated fibroblasts, and as a result, promote the repair process in normal tissues damaged by irradiation. Thus, CA may be a good therapeutic target, not only to inhibit the invasive ability of IR cancer cells but also to promote the fibroblast-mediated repair process in normal tissues.

In summary, high-invasive IR cells demonstrated invasive activity dependent on the phosphorylation level of MRLC. PP-MRLC inhibited the invasive phenotype in IR cells, while dephosphorylation of MRLC induced an invasive phenotype in low-invasive P-3 cells. Thus, MRLC is a possible therapeutic target for invasive lung adenocarcinoma.

**Acknowledgments**

This study was supported by Grants-in-Aid for JSPS Fellows (11J06280) to I.S., Scientific Research (A) (21249065) to H.S. and H.H., Scientific Research (B) (24390285) to M.Y., T.N. and H.H., Scientific Research on Innovative Areas (24106502) to T.M., and Exploratory Research (23651099) to K.K. from the Ministry of Education, Culture, Sports, Science and Technology, Japan.

**REFERENCES**

- [1] von Essen, C.F. (1991). Radiation enhancement of metastasis: a review. *Clin. Exp. Metastasis*. 9, 77-104.
- [2] Tsutsumi, K., Tsuda, M., Yazawa, N., Nakamura, H., Ishihara, S., Haga, H., Yasuda, M., Yamazaki, R., Shirato, H., Kawaguchi, H., Nishioka, T., Ohba, Y. (2009). Increased motility and invasiveness of tumor cells that survived 10 Gy irradiation. *Cell Struct. Funct.* 34, 89-96.
- [3] Tsukamoto, H., Shibata, K., Kajiyama, H., Terauchi, M., Nawa, A., Kikkawa, F. (2007). Irradiation-induced epithelial-mesenchymal transition (EMT) related to invasive potential in endometrial carcinoma cells. *Gynecol. Oncol.* 107, 500-504.
- [4] Cordes, N., Blaese, M. A., Meineke, V., van Beuningen, D. (2002). Ionizing radiation induces up-regulation of functional  $\beta$ 1-integrin in human lung tumour cell lines *in vitro*. *Int. J. Radiat. Biol.* 78, 347-357.
- [5] Cordes, N., Hansmeier, B., Beinke, C., Meineke, V., van Beuningen, D. (2003). Irradiation differentially affects substratum-dependent survival, adhesion, and invasion of glioblastoma cell lines. *Brit. J. Cancer.* 89, 2122-2132.
- [6] Nishioka, T., Yasuda, M., Tsutsumi, K., Haga, H., Shirato, H. (2007). Matrixmetalloproteinases: up-regulated in subclones that survived 10-Gy irradiation. *Radiat. Med.* 25, 430-431.

[7] Mizutani, T., Haga, H., Koyama, Y., Takahashi, M., Kawabata, K. (2006).

Diphosphorylation of the Myosin Regulatory Light Chain Enhances the Tension Acting on Stress Fibers in Fibroblasts. *J. Cell. Physiol.* 209, 726-731.

[8] Yamazaki, D., Kurusu, S., Takenawa, T. (2005). Regulation of cancer cell motility through actin reorganization. *Cancer Sci.* 96, 379-386.

[9] Ridley, A. J. (2001). Rho GTPases and cell migration. *J. Cell. Sci.* 114, 2713-2722

[10] Ishihara, S., Haga, H., Yasuda, M., Mizutani, T., Kawabata, K., Shirato, H., Nishioka, T. (2010). Integrin  $\beta$ 1-dependent invasive migration of irradiation-tolerant human lung adenocarcinoma cells in 3D collagen matrix. *Biochem. Biophys. Res. Commun.* 396, 651-655.

[11] Ishihara, H., Martin, B. L., Brautigan, D. L., Karaki, H., Ozaki, H., Kato, Y., Fusetani, N., Watabe, S., Hashimoto, K., Uemura, D., Hartshorne, D. J. (1989). CalyculinA and okadaic acid: inhibitors of protein phosphatase activity. *Biochem. Biophys. Res. Commun.* 159, 871-877.

[12] Hall, D.E., Reichardt, L.F., Crowley, E., Holley, B., Moezzi, H., Sonnenberg, A., Damsky, C.H. (1990). The  $\alpha$ 1/ $\beta$ 1 and  $\alpha$ 6/ $\beta$ 1 integrin heterodimers mediate cell attachment to distinct sites on laminin. *J. Cell Biol.* 110, 2175-2184.

[13] Friedl, P. and Wolf, K. (2010). Plasticity of cell migration: a multiscale tuning model. *J. Cell Biol.* 188, 11-19.

[14] Wolf, K., Mazo, I., Leung, H., Engelke, K., von Andrian, U. H., Deryugina, E. I., Strongin,

A. Y., Bröcker, E-B., Friedl, P. (2003). Compensation mechanism in tumor cell migration: mesenchymal-amoeboid transition after blocking of pericellular proteolysis. *J. Cell Biol.* 160, 267-277.

[15] Itoh, K., Yoshioka, K., Akedo, H., Uehata, M., Ishizaki, T., Narumiya, S. (1999). An essential part for Rho-associated kinase in the transcellular invasion of tumor cells. *Nat. Med.* 5, 221-225.

[16] Dormand, E-L., Banwell, P. E., Goodacre, T. EE. (2005). Radiotherapy and wound healing. *Int. Wound J.* 2, 112-127.

[17] Gieringer, M., Gosepath, J., Naim, R. (2011). Radiotherapy and wound healing: principles, management and prospects (review). *Oncol. Rep.* 26, 299-307.

[18] Petrie, R. J., Gavara, N., Chadwick, R. S., Yamada, K. M. (2012). Nonpolarized signaling reveals two distinct modes of 3D cell migration. *J. Cell Biol.* 197, 439-455.

[19] Nobe, H., Nobe, K., Fazal, F., De Lanerolle, P., Paul, R. J. (2003). Rho kinase mediates serum-induced contraction in fibroblast fibers independent of myosin LC20 phosphorylation. *Am. J. Physiol. Cell Physiol.* 284, C599-C606.

**FIGURE LEGENDS****Fig. 1**

(A) Fluorescent images of F-actin and diphosphorylated MRLC (PP-MRLC) in cells cultured in a 3D collagen gel. P-3: subclonal A549 cells, IR: irradiation-tolerant cells derived from P-3 cells. Cross-sectional views of XZ and YZ directions (axes) are shown together. Bar = 20  $\mu\text{m}$ . (B) Fluorescent intensity of PP-MRLC/F-actin ratio in P-3 and IR cells. The mean values of 20 cells are shown with SD (shown as error bars) calculated from 3 independent experiments. \*P < 0.01.

**Fig. 2**

(A) Fluorescent images of F-actin in P-3 cells treated with Y27632 and cultured in a 3D collagen gel. Bar = 30  $\mu\text{m}$ . (B) The proportion of cell morphology categorized as round or spindle-shaped. The mean values of more than 150 cells are shown with SD (shown as error bars) calculated from at least 3 independent experiments. \*P < 0.05. (C) Fluorescent images of F-actin in IR cells treated with calyculin A (CA) and cultured in a 3D collagen gel. Bar = 30  $\mu\text{m}$ . (D) The proportion of cell morphology categorized as round or spindle-shaped. The mean values of more than 150 cells are shown with SD (shown as error bars) calculated from at least 3 independent experiments. \*P < 0.05.

**Fig. 3**

Time-lapse phase contrast observation of cells cultured in a 3D collagen gel. IR: IR cells, IR + CA: IR cells treated with calyculin A (CA), IR + CA + washout: IR cells after washout of CA. Numbers on the images indicate the relative time from the start of the observation. The white arrow shows the direction of cell movement. Bar = 50  $\mu\text{m}$ .

**Fig. 4**

(A) Fluorescent images of F-actin in P-3 cells, P-3 cells treated with only Y27632, or P-3 cells treated with both Y27632 and AIB2, cultured in a 3D collagen gel. Bar = 30  $\mu\text{m}$ . (B) The proportion of cell morphology categorized as round or spindle-shaped. The mean values of more than 150 cells are shown with SD (shown as error bar) calculated from at least 3 independent experiments. \* $P < 0.05$ .

**SUPPLEMENTARY MATERIALS****Fig. S1**

(A) Fluorescent images of F-actin and diphosphorylated MRLC (PP-MRLC) in P-3 cells treated with Y27632 and cultured in a 3D collagen gel. Cross-sectional views of XZ and YZ directions (axes) are shown together. Bar = 20  $\mu\text{m}$ . (B) Fluorescent intensity of PP-MRLC/F-actin ratio in P-3 cells and P-3 cells treated with Y27632. The mean values of 20 cells are shown with SD (shown as error bars). \* $P < 0.01$ .

**Fig. S2**

(A) Fluorescent images of F-actin and diphosphorylated MRLC (PP-MRLC) in IR cells, IR cells treated with DMSO, and IR cells treated with calyculin A (CA), and cultured in a 3D collagen gel. Cross-sectional views of XZ and YZ directions (axes) are shown together. Bar = 20  $\mu\text{m}$ . (B) Fluorescent intensity of PP-MRLC/F-actin ratio in IR cells, IR cells treated with DMSO, and IR cells treated with CA. The mean values of 12 cells are shown with SD (shown as error bars). \* $P < 0.01$ .

**Fig. S3**

(A) Fluorescent images of F-actin in P-3 cells treated with only Y27632 or P-3 cells treated with both Y27632 and IgG control antibody, cultured in a 3D collagen gel. Bar = 30  $\mu\text{m}$ . (B) The proportion of cell morphology categorized as round or spindle-shaped. The mean values of more than 150 cells are shown with SD (indicated by the error bars) calculated from at least 3 independent experiments.

**Movie**

Time-lapse phase contrast observations of IR cells cultured in a 3D collagen gel. IR cells were observed for 12 h (untreated condition). After observation, the cells were treated with calyculin A (CA) and observed for 12 h. After removing CA, the cells were then observed for 27 h. Video time, 1 second = real time, 60 minutes; bar = 20  $\mu\text{m}$ .

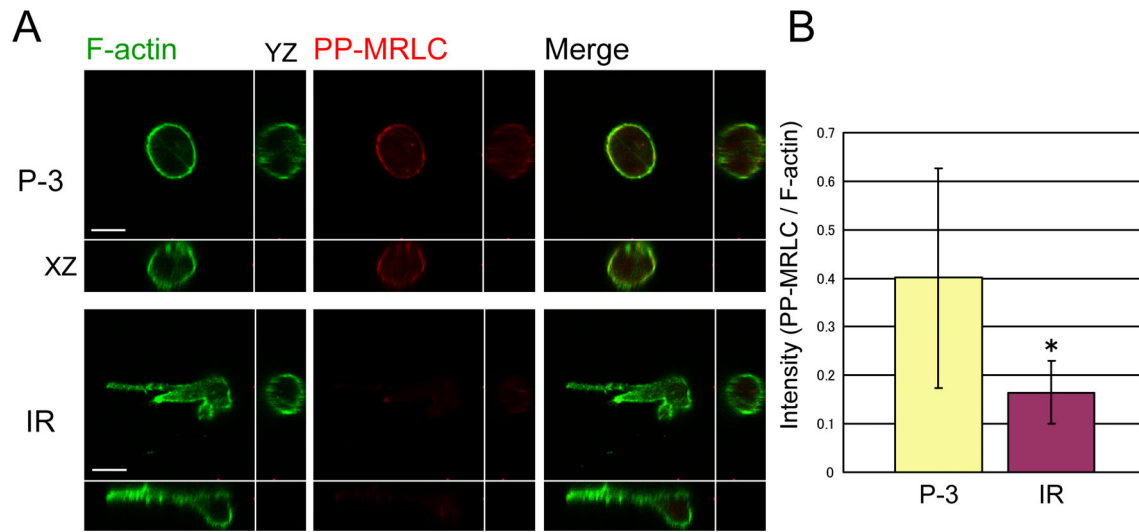


Fig. 1. S. Ishihara *et al.*

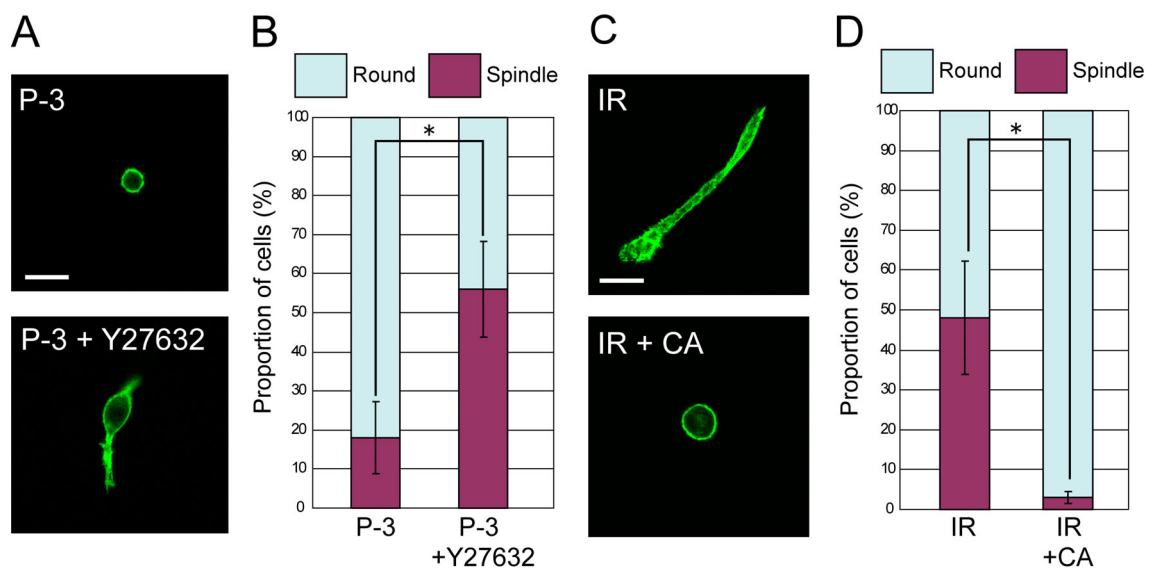


Fig. 2. S. Ishihara *et al.*

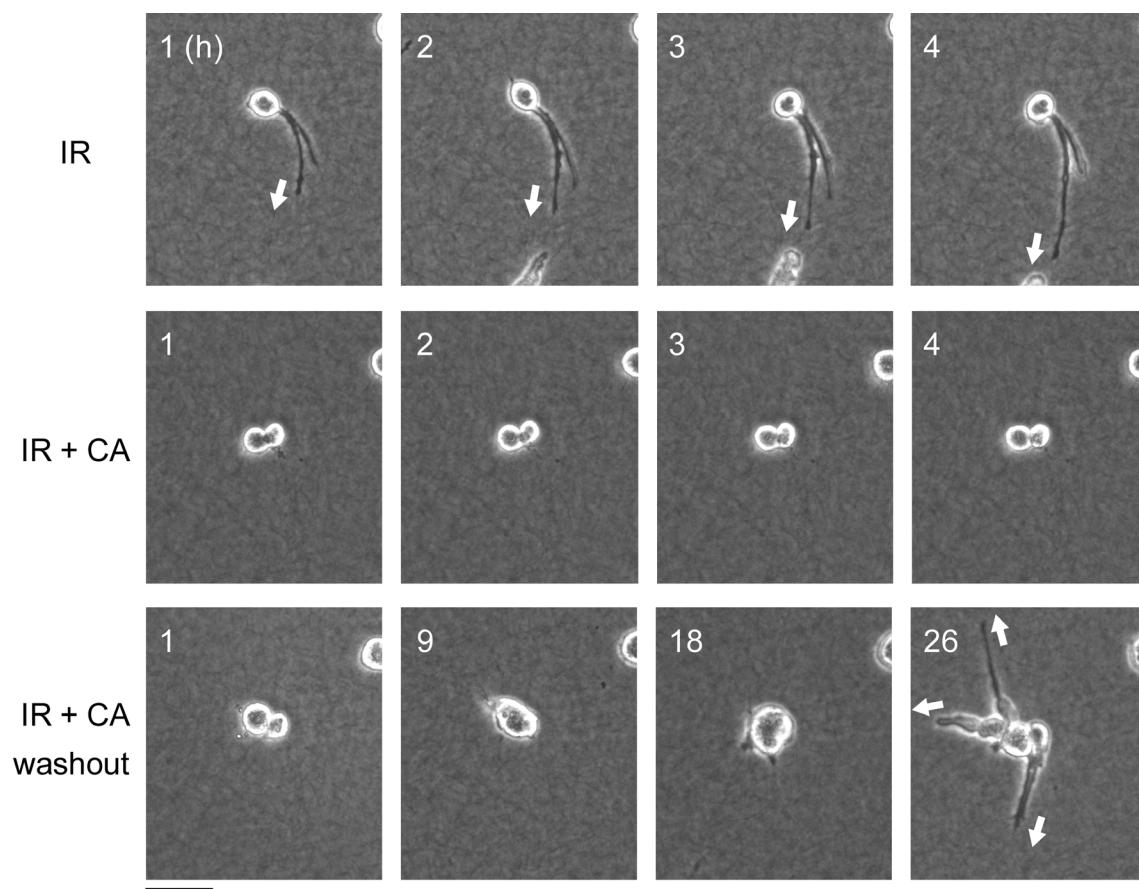


Fig. 3. S. Ishihara *et al.*

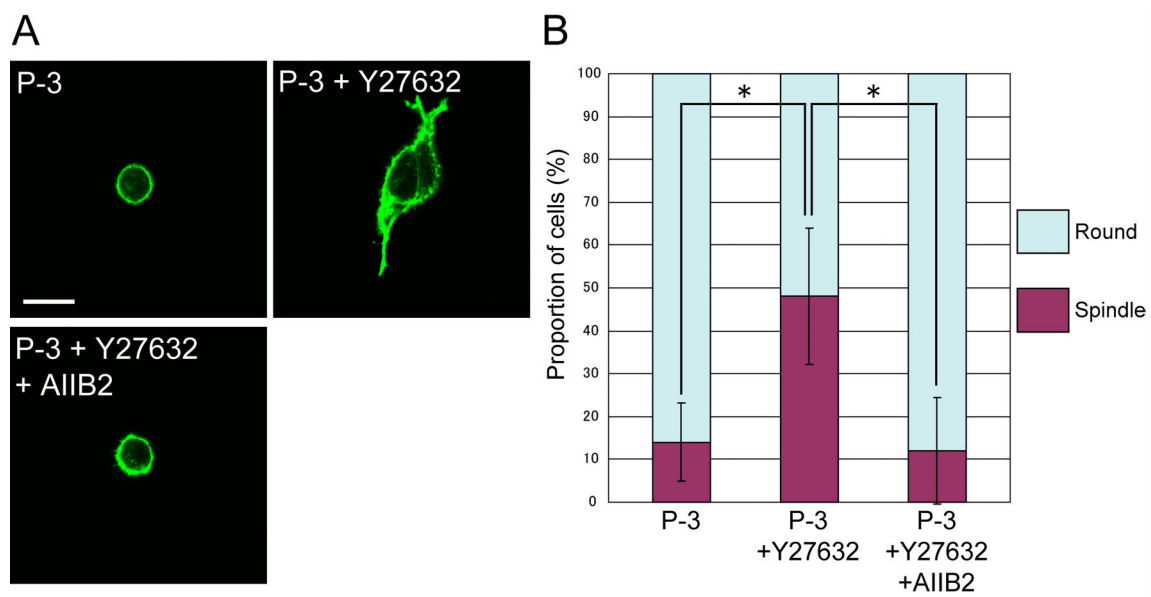


Fig. 4. S. Ishihara *et al.*

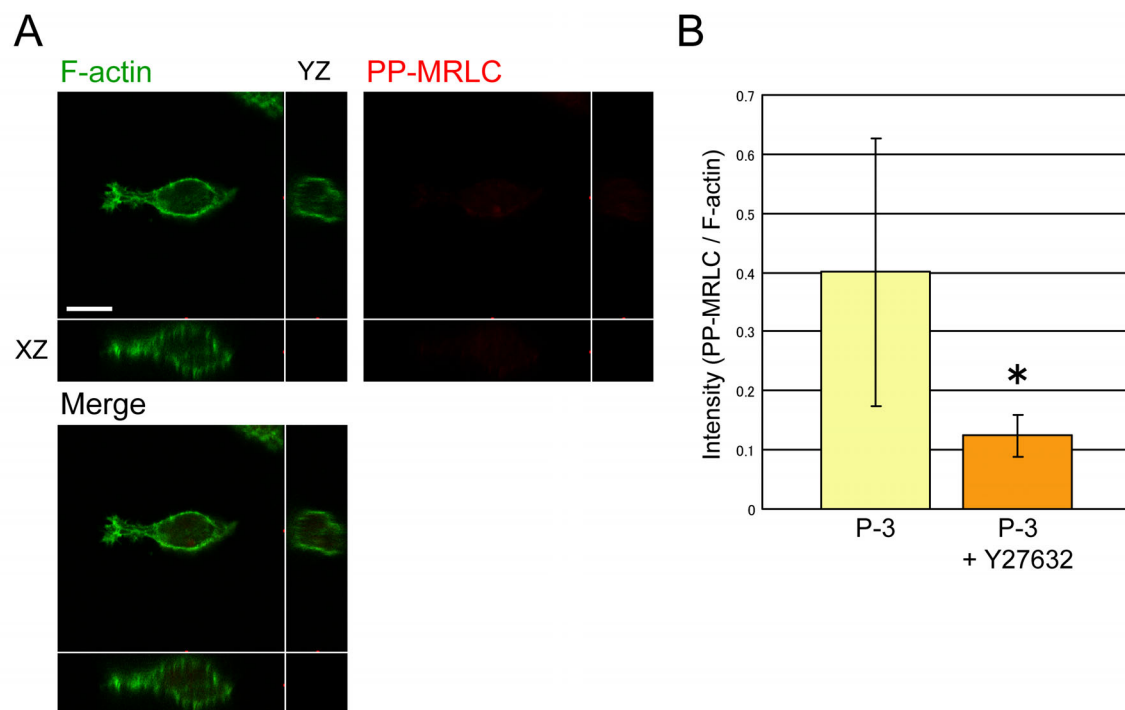
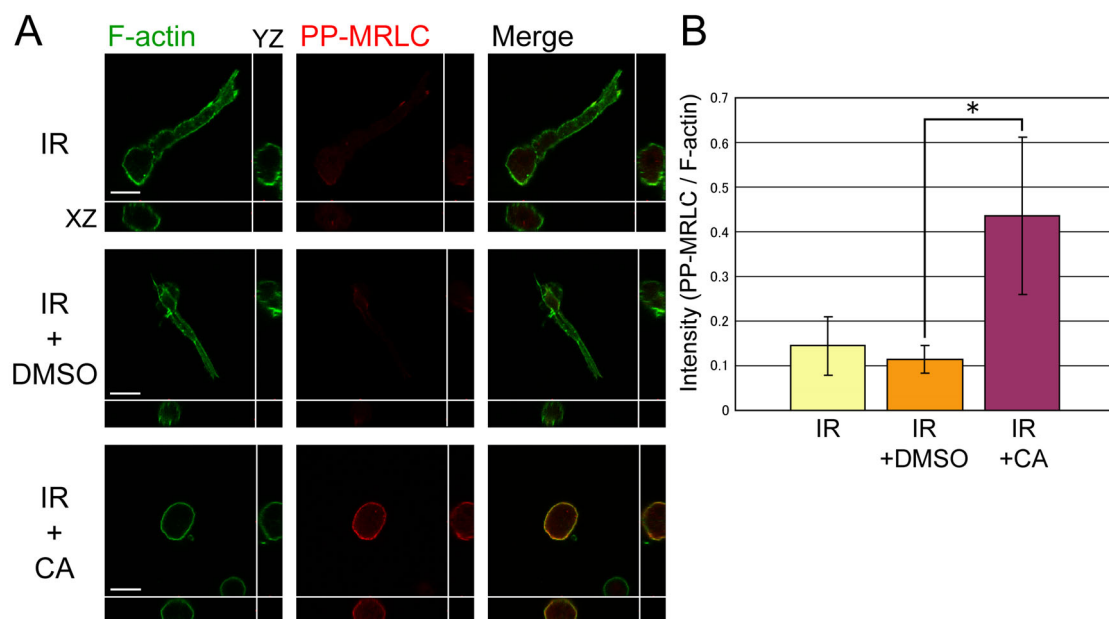
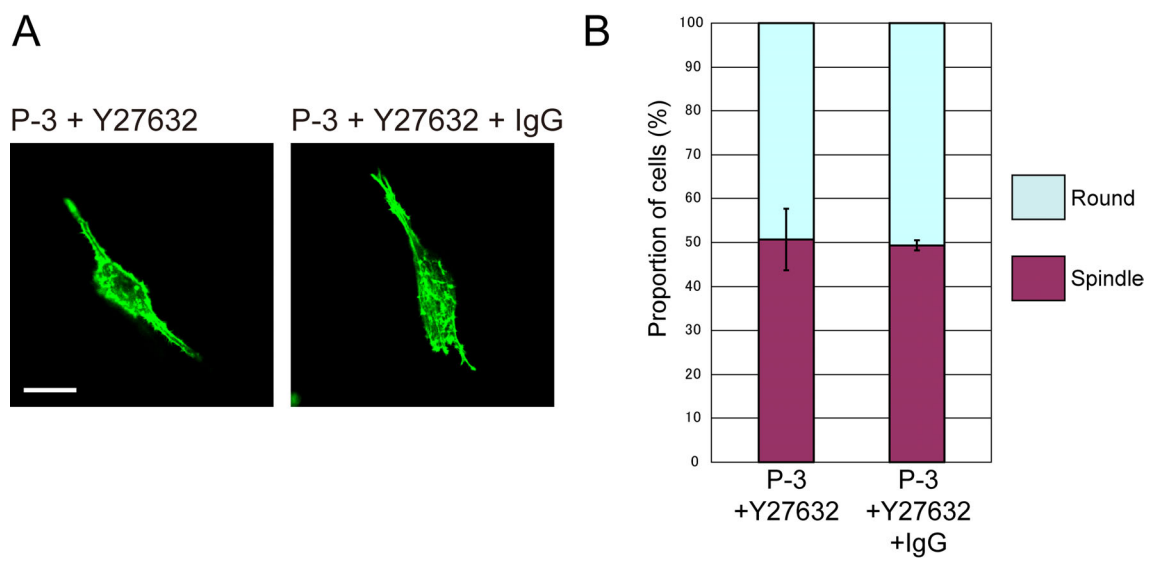


Fig. S1. S. Ishihara *et al.*

Fig. S2 S. Ishihara *et al.*

Fig. S3 S. Ishihara *et al.*